A Robust Ion-Conductive Biopolymer as a Binder for Si Anodes of Lithium-Ion Batteries

Jie Liu, Qian Zhang, Tao Zhang, Jun-Tao Li, Ling Huang, and Shi-Gang Sun**

Binders have been reported to play a key role in improving the cycle performance of Si anode materials of lithium-ion batteries. In this study, the biopolymer guar gum (GG) is applied as the binder for a silicon nanoparticle (SiNP) anode of a lithium-ion battery for the first time. Due to the large number of polar hydroxyl groups in the GG molecule, a robust interaction between the GG binder and the SiNPs is achieved, resulting in a stable Si anode during cycling. More specifically, the GG binder can effectively transfer lithium ions to the Si surface, similarly to polyethylene oxide solid electrolytes. When GG is used as a binder, the SiNP anode can deliver an initial discharge capacity as high as 3364 mAh g^{-1}, with a Coulombic efficiency of 88.3% at the current density of 2100 mA g^{-1}, and maintain a capacity of 1561 mAh g^{-1} after 300 cycles. The study shows that the electrochemical performance of the SiNP anode with GG binder is significantly improved compared to that of a SiNP anode with a sodium alginate binder, and it demonstrates that GG is a promising binder for Si anodes of lithium-ion batteries.

1. Introduction

Lithium-ion batteries (LIBs), with their high energy density, are one of the most promising energy storage devices to address the increasing energy storage demands for various technological applications, including portable electronic devices, electric vehicles (EVs) and hybrid electric vehicles (HEVs).[1,2] However, the commercial graphite anode has severely impeded the application of LIBs in EVs and HEVs, due to its low theoretical capacity of 372 mAh g^{-1}. Si, however, exhibits a high theoretical capacity of 4200 mAh g^{-1} and has attracted significant attention as an anode material in LIBs.[1–3] Unfortunately, the practical application of Si anode materials in LIBs is still quite challenging. Large variation in volume occurs during charge–discharge cycling, which causes fracturing and pulverization of the Si anode materials and breaks the electrical contacts between active Si materials and conductive additives, resulting in a rapid capacity fading and a short cycle life.[2–4]

One of the main approaches is adopting nanostructured Si materials to reduce the volume change and, thus, the pulverization of active Si materials.[4–11] Unfortunately, composite electrode films still fracture due to the intrinsic volume change of Si materials during cycling, leading to limited cycle lifes. Therefore, robust binders are required to stabilize the structure of the electrode and to explore the applications of nanostructured Si anode materials. Recent studies have demonstrated that numerous important battery characteristics, including cycle stability and irreversible capacity loss, are strongly dependent on the properties of the binder.[1–3,12–15] Polyacrylic acid (PAA), carboxymethyl cellulose (CMC), and sodium alginate (SA) have been used as binders to enhance the electrochemical properties of Si anodes, utilizing the hydrogen bonds forming between the silicon oxide layers on Si surfaces and the polar functional groups of the binders.[13–15] However, to further improve the electrochemical performances of Si anode materials, modified binders and new polymer binders are still required. Ryou et al. prepared mussel-inspired adhesive binders through conjugation of dopamine hydrochloride to SA and PAA to obtain high-capacity Si anodes.[12] We developed an alginate hydrogel binder with improved mechanical strength by cross-linking reaction between SA and Ca^{2+} ions to enhance the cycle stability of a Si/C anode.[16] Song et al. synthesized an interpenetrated gel polymer binder with deformable polymer network and strong adhesion through in situ cross-linking of PAA and polyvinyl alcohol (PVA).[17] Liu et al. synthesized electroconductive polymers as binders to achieve high-performance Si-based anodes.[18,19]

However, it should be mentioned that the above reports focus on improving the mechanical properties and electrical conductivity of the polymer binders, while the lithium-ion conduction in polymer binders is rarely considered. Due to the large coverage of the Si anode material surface by the binder, the binder is required to provide access for lithium ions to reach the Si surface in order to achieve a high-capacity Si anode. It has been reported that polyethylene oxide (PEO)-based solid polymer electrolytes can effectively transfer lithium ions, due to the lone-pair electrons on the oxygen of the ether groups, which

J. Liu, Prof. L. Huang, Prof. S.-G. Sun
State Key Laboratory of Physical Chemistry of Solid Surfaces
College of Chemistry and Chemical Engineering
Xiamen University
Xiamen 361005, P.R. China
E-mail: sgsun@xmu.edu.cn
Q. Zhang, T. Zhang, Dr. J.-T. Li
College of Energy
Xiamen University
Xiamen 361005, P.R. China
E-mail: jtli@xmu.edu.cn

DOI: 10.1002/adfm.201500589

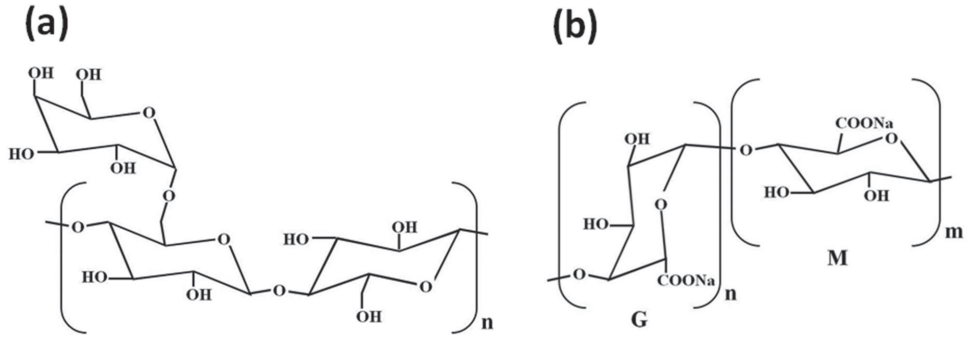

Figure 1. Chemical structures of guar gum (GG) (a) and sodium alginate (SA) (b).

can coordinate lithium ions: The complex lithium ions can then move between complexation sites assisted by the segmental motion of the polymer matrix.[20–24] Guar gum (GG) is a polysaccharide derived from the seeds of *Cyamopsis tetragonolobus* and consists of linear chains of (1→4)-β-D-mannopyranosyl units with α-D-galactopyranosyl units attached through (1→6) linkages,[25–27] illustrated schematically in **Figure 1**a. It has been reported that GG can transfer lithium ions similarly to PEO polymer electrolytes and could be used to prepare gel polymer electrolytes for supercapacitors.[28]

Considering the ion-conductivity and the large amounts of polar hydroxyl groups in the GG molecule, GG was chosen and applied as a promising binder for Si-based anodes of LIBs for the first time in this study. We demonstrate that the electrochemical performance of a Si nanoparticle (SiNP) anode is significantly improved by the GG binder in comparison to the SA binder. Thus, the GG binder provides a new binder-design perspective for Si anodes of LIBs.

2. Results and Discussion

The interaction between binder and active Si material is one of the most critical factors that affect the cycle performance of Si-based anodes.[15] Figure 1a and b display the chemical structures of GG and SA, respectively. More polar hydroxyl groups can be observed in the GG molecule, which result in a larger number of possible binder–Si bonds. Therefore, the GG binder is likely to show a more robust interaction with active Si materials and, thus, be a promising binder for Si-based anodes. Figure S1a in the Supporting Information indicates that the GG binder shows a significantly higher viscosity (5600 mPa s) than the SA binder (1520 mPa s). As a result, composite electrode films with a GG binder could be tightly attached to the current collector, even in the presence of large volume change, which is the precondition for repeatable battery operation. It has been reported that the stiff nature of the SA backbone contributes to the stability of the electrode structure.[12,15] Fortunately, the GG binder is even harder than the SA binder, as displayed in Figure S1b. Therefore, the robust GG binder is expected to show preferable electrochemical performance.

To investigate the formation of the polar hydrogen bonds between the GG binder and the active Si material, Fourier transform infrared (FTIR) spectra have been recorded. If an interaction takes place in the material, the peak assigned to a specific functional group in the FTIR spectrum shifts to either a higher or a lower wavenumber, or a new peak (or shoulder) arises in the spectrum.[3] **Figure 2**a shows that pure GG shows a broad absorption band at 3446 cm^{-1} ascribed to the stretching of O–H, a peak at 1159 cm^{-1} corresponding to a C–OH stretching mode, and a peak at 1089 cm^{-1} corresponding to the stretching of CH_2–OH.[27,29] After mixing with SiNPs, the bands assigned to O–H, C–OH, and CH_2–OH obviously shift to lower wavenumbers at 3418, 1144, and 1074 cm^{-1}, respectively, demonstrating that an interaction occurs between the GG binder and the SiNPs. Previous literature reports have shown that SiNPs are covered by SiO_x layers with many hydroxyl groups (silanol groups).[3,17,30] The silanol groups can form hydrogen bonds with the hydroxyl groups of the GG molecule. As a consequence, a small amount of electron density is transferred from the proton acceptor (O) to the proton donor (O–H), resulting in a weakening of the O–H bond. This weakening is accompanied

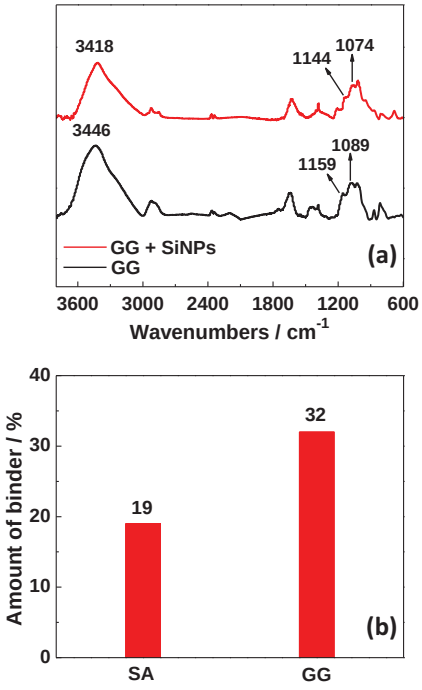

Figure 2. a) FTIR spectra of pure GG and a Si/GG blend. b) The remaining amounts of binders calculated from TGA before and after washing the Si/binder blends with water.

by bond elongation and a concomitant decrease of the O–H stretch vibration frequency.[31] At the same time, the electron density of the oxygen atom also changes and weakens the C–O bond. Thus, the bands ascribed to O–H, C–OH, and CH_2–OH shift to lower wavenumbers.

To study the binding strength between the GG binder and the SiNPs, thermogravimetric analysis (TGA) has been carried out. Choi and co-workers have used TGA to assess the binding strength between a hyperbranched β-cyclodextrin polymer binder and SiNPs.[1] The TGA results reveal that the remaining amounts of GG binder and SA binder are 32% and 19% of the original amounts after the same washing step (Figure 2b and Figure S2), respectively. The larger remaining amount of binder after washing demonstrates the stronger interaction between the GG binder and SiNPs. The more robust interaction is due to the larger number of polar hydroxyl groups in the GG molecule, which provides more possible sites to form hydrogen bonds. Therefore, the GG binder can effectively bind SiNPs on the current collector and maintain an integrated conductive network during cycling, as shown in Figure S3.

Pure SiNPs were used as active material to evaluate their electrochemical performance. The scanning electron microscopy (SEM) and transmission electron microscopy (TEM) images in **Figure 3** show that the SiNPs are of spherical shape with an average size of about 100 nm and exhibit a Brunauer–Emmett–Teller (BET) specific surface area of 27.4 $m^2\ g^{-1}$. The powder X-ray diffraction (XRD) pattern in Figure 3c reveals the crystal structure of the SiNPs. **Figure 4** displays the cycle performance of SiNP anodes with different binders. Figure 4a and b show that the SiNP anode with GG binder delivers an initial discharge capacity of 3364 mAh g^{-1} with a high initial Coulombic efficiency of 88.3% at a current density of 2100 mA g^{-1}. After 100 charge–discharge cycles the SiNP anode still holds a high capacity of 2222 mAh g^{-1}. In contrast, the SiNP anode with SA binder shows an initial discharge capacity of only 2195 mAh g^{-1} and an initial Coulombic efficiency of 82.5%. The discharge capacity decreases to 1377 mAh g^{-1} after 100 charge–discharge cycles. The SiNP anode with PVDF binder shows a very poor cycle performance with an initial discharge capacity of only 1232 mAh g^{-1} and a rapid capacity loss.

The poor cycle performance of the SiNP anode with PVDF binder is mainly due to the weak Van der Waals interactions between the PVDF binder and SiNPs, which cannot accommodate the huge volume variation of the SiNPs during charge–discharge cycling. This leads to a degradation of the electrical conduction network, an isolation of the SiNPs, and, finally, capacity fading. The superior cycle properties of SiNP electrodes with GG binder and SA binder are ascribed to the stronger hydrogen bonds as well as the stiff nature of the binders' backbones. However, although both GG binder and SA binder can form hydrogen bonds with SiNPs, the SiNP anode with GG binder delivers a much higher capacity. **Figure 5**a shows the CV

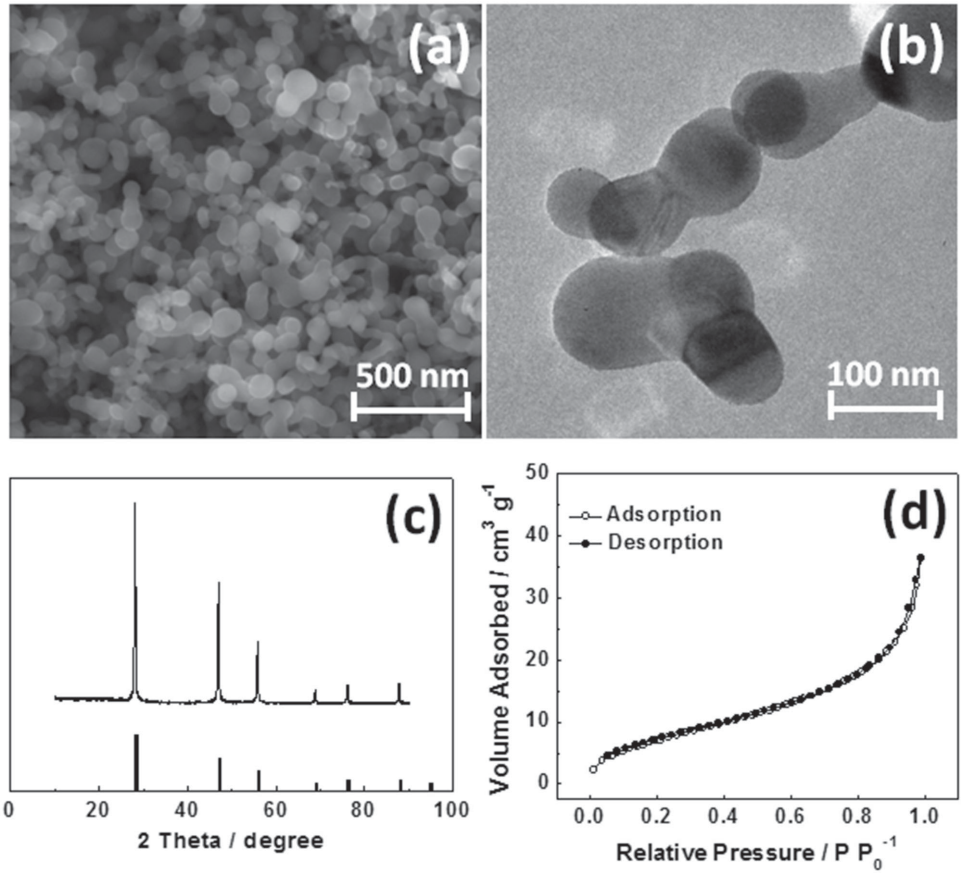

Figure 3. a) SEM image, b) TEM image, c) XRD spectrum, and d) N_2 adsorption and desorption isotherms of the SiNPs.

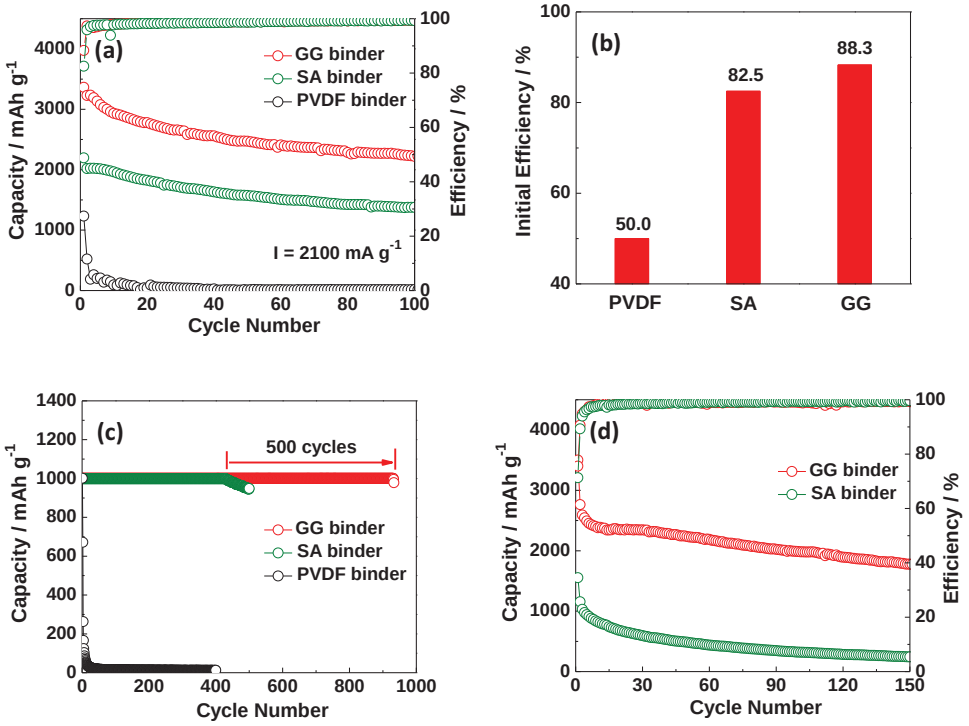

Figure 4. Electrochemical performance of SiNP anodes with different binders. a) Cycle performance at 2100 mA g^{-1} between 0.01 and 1.2 V; b) initial efficiency at 2100 mA g^{-1}; c) cycle performance with limited discharge capacity of 1000 mAh g^{-1} at 1000 mA g^{-1}; d) cycle performance at 630 mA g^{-1} between 0.01 and 1.2 V with a low binder ratio of 15%.

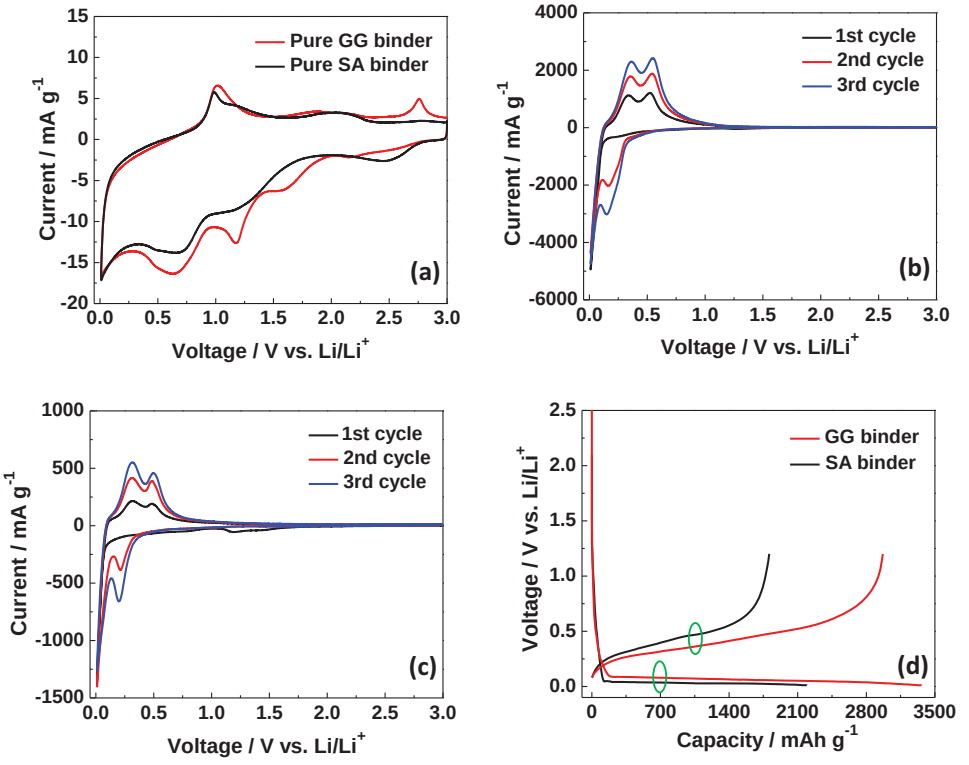

Figure 5. a) CV curves of the pure SA binder and GG binder at a scanning rate of 0.2 mV s^{-1}; CV curves of SiNP anodes with b) GG binder and c) SA binder at a scanning rate of 0.2 mV s^{-1}; d) charge–discharge curves of SiNP anodes with SA binder and GG binder at 2100 mA g^{-1}.

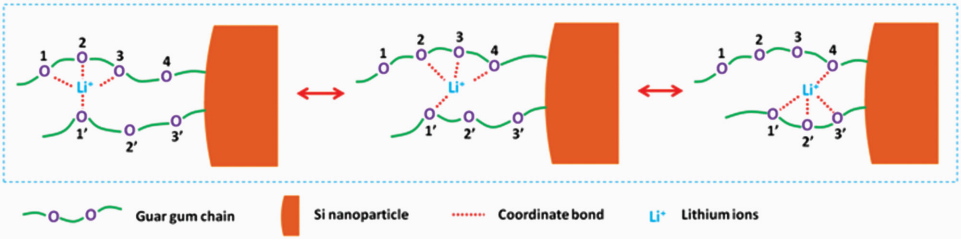

Figure 6. Schematic illustration of lithium-ion transfer in the GG binder. Lithium-ion transport is described as the motion of the lithium ions between complexation sites, assisted by the segmental motion of the GG binder.

curves of pure GG binder and SA binder, which reveal that both binders are electrochemically inactive between 0.01 and 3.0 V, indicated by the very weak oxidation–reduction current. Thus, the capacity of the binders compared to the capacity of the whole electrode is negligible. The robust contact between the GG binder and SiNPs resulting from the large number of hydrogen bonds promotes the stability of an integrated electrical conduction network within the electrode. As a consequence, the amount of isolated Si decreases, which contributes to a higher capacity.[3,12] More specifically, the lone-pair electrons of the oxygen heteroatoms in the GG molecule can coordinate with the lithium ions. The complex lithium ions will dissociate from their complexation sites due to the thermal motion of the GG molecule and conjugate with new sites, leading to a motion of lithium ions, as shown in **Figure 6**, similarly to that in PEO solid electrolytes.[28] Due to the complexation between the oxygen heteroatoms in the GG molecule and the cations, GG has been applied as a corrosion inhibitor for carbon steel in sulfuric acid solution and mild steel in hydrochloric acid solution.[32,33] The effective lithium-ion conduction of the GG binder decreases the polarization of the SiNP electrode and, thus, improves the capacity of the SiNP anode, as discussed later.

The higher initial Coulombic efficiency of the SiNP anode with the GG binder can be explained as follows: Firstly, the formation of more hydrogen bonds between the SiNPs and the GG binder effectively restrains irreversible movement of the SiNPs and maintains electrical contacts between the SiNPs and the conductive additive, leading to a decrease in isolated Si during the first charge–discharge cycle. Secondly, the CV curves of SiNP anodes with GG and SA binders, shown in Figure 5b and c, reveal a peak associated with the formation of the solid–electrolyte interphase (SEI) film in the first cathodic scan of the SiNP anode with SA binder at about 1.25 V, whereas a corresponding peak of the SiNP anode with GG binder is difficult to distinguish. The larger number of hydroxyl groups in the GG molecule provides more contact points between the SiNPs and the GG binder, ensuring a better coverage of the SiNP surfaces, which decreases the contact between the SiNPs and the electrolyte and, thus, the decomposition of the electrolyte at the SiNP surfaces. Electrochemical impedance spectroscopy (EIS) results, shown in Figure S4, also demonstrate the reduced decomposition of electrolyte at the surfaces of the SiNP anode with GG binder, indicated by the smaller size of the semicircle in the high-frequency range, which is assigned to the SEI resistance.[34] Moreover, during stable cycling, the SiNP anode with GG binder also shows a higher Coulombic efficiency, due to the robust contact between the GG binder and the SiNPs. The Coulombic efficiency of the SiNP anode with GG binder can reach 97.3% at the second cycle and 99.5% at the 100th cycle, whereas, the Coulombic efficiency of the SiNP anode with SA binder is only 95.9% at the second cycle and 99.3% at the 100th cycle.

Figure 4c displays the cycle performance of SiNP anodes with a lithium insertion capacity limited to 1000 mAh g^{-1} at 1000 mA g^{-1}. The whole SiNP electrode, with GG binder or SA binder, undergoes a similar volume change due to the same capacity limitation. It shows that the SiNP anode with SA binder can hold the capacity of 1000 mAh g^{-1} for 430 cycles, whereas, the SiNP anode with GG binder can perform 930 cycles with the capacity of 1000 mAh g^{-1}. The significantly longer cycle life of the SiNP anode with GG binder indicates that the larger number of polar functional groups in the GG molecule provides more possible sites to form binder–Si bonds, which ensures a more robust interaction between the binder and the SiNPs and, thus, a more stable electrode structure. In a real cycle performance test between 0.01 and 1.2 V, the SiNP anode with GG binder can also keep a high capacity of 1561 mAh g^{-1} after long-term charge–discharge cycling (300 cycles) at 2100 mA g^{-1}, as shown in Figure S5, owing to the robust interaction between the GG binder and the SiNPs. Figure S6 demonstrates that a SiNP anode with GG binder and a high SiNP loading of 1.1 mg cm^{-2} also shows a high capacity and good cycle stability without rapid capacity fading. Even with a low binder ratio of 15%, the SiNP anode with GG binder still shows superior cycle performance with a capacity of 1779 mAh g^{-1} after 150 cycles at 630 mA g^{-1}, as shown in Figure 4d. In contrast, the SiNP anode with SA binder shows low capacity and poor cycle performance. The superior rate performance with much higher capacity at each current density of the SiNP anode with GG binder, displayed in Figure S7, due to the effective lithium-ion conduction and strong interaction between the GG binder and the SiNPs, demonstrates that GG is a promising binder for Si anodes. Recently, GG has been successfully used as a binder for a $Li_4Ti_5O_{12}$ electrode, and shows much better electrochemical performance than a CMC binder,[35] which has a similar structure to SA.

The charge–discharge curves of SiNP anodes with GG binder and SA binder are shown in Figure 5d. Similar curves are observed with a long and flat discharge plateau below 0.10 V, ascribed to the insertion of lithium ions into Si, and a slant charge plateau from 0.25 to 0.65 V, ascribed to the extraction of lithium ions from the Li_xSi phase. Interestingly, the polarization of the electrode with GG binder obviously drops, demonstrated by the lower charge plateau and higher discharge plateau. The decreased polarization reveals that the oxygen

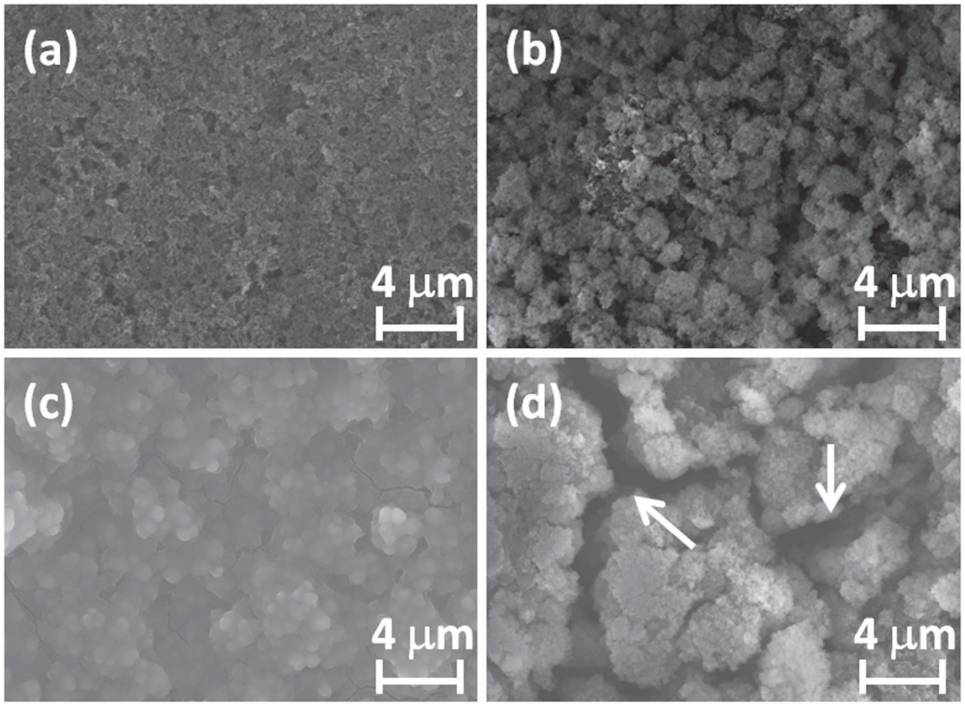

Figure 7. SEM images of SiNP electrodes a,b) before cycling with GG binder (a) and SA binder (b) and c,d) after 400 cycles with limited discharge capacity of 1000 mAh g^{-1} at 1000 mA g^{-1} with GG binder (c) and SA binder (d). The white arrowheads in (d) point to cracks.

heteroatoms in the GG molecule provide complexation sites, thus, transport pathways for lithium ions, leading to superior lithium-ion conduction. The CV curves of the SiNP anodes with GG binder and SA binder, displayed in Figure 5b and c, also show the same result. The larger peak current of the SiNP anode with GG binder demonstrates the higher reaction activity of the electrode. As alloying and dealloying reactions of Si with lithium ions are the same on the SiNP anodes with GG binder and SA binder, the higher reaction activity of the electrode with GG binder is mainly due to the superior lithium-ion conduction, which decreases the polarization of the electrode. EIS results, shown in Figure S4, also demonstrate the smaller charge–transfer resistance of the SiNP electrode with GG binder, indicated by the smaller size of the semicircle in the medium-frequency range.

Figure 7 compares the SEM images of SiNP electrodes with GG binder and SA binder. Figure 7a and b display the SEM images of the SiNP anodes before cycling. The electrode with SA binder shows a conglobate morphology, while the electrode with GG binder displays a uniform structure. The high viscosity of the GG binder prevents the SiNPs from sedimentation and aggregation during the electrode formation, leading to a high slurry uniformity, which is important to obtain a superior long-term cycle performance.[15] After 400 charge–discharge cycles with limited discharge capacity of 1000 mAh g^{-1} at 1000 mA g^{-1}, pulverization and cracks are observed on the electrode with SA binder (Figure 7d), due to the relatively weak interaction between the SA binder and the SiNPs. However, the electrode with GG binder can maintain an integrated electrode structure without pulverization (Figure 7c), owing to the more robust interaction between the GG binder and the SiNPs as well as the stronger mechanical properties of the GG binder, which can effectively accommodate the large volume variation of the SiNPs during cycling.

3. Conclusion

In this study, GG has been successfully applied as a high-performance binder for a Si anode of a LIB for the first time. The GG binder shows more robust mechanical properties with a 3.7 times higher viscosity and a 1.6 times higher hardness than those of the SA binder. The larger number of polar functional groups in the GG molecule provides more possible sites to form binder–Si bonds, leading to a more robust interaction between the GG binder and the Si anode material. More specifically, the GG binder can provide transport pathways for lithium ions to ensure superior lithium-ion conduction during charge–discharge processes, similarly to those in PEO solid electrolytes. Thus, the mechanically robust and ion-conductive GG is a promising binder for Si anodes of LIBs. At a current density of 2100 mA g^{-1}, the SiNP anode with GG binder delivers a capacity of 2222 mAh g^{-1} after 100 charge–discharge cycles, which is much higher than that of a SiNP anode with SA binder (1377 mAh g^{-1}). When the whole electrode undergoes a similar volume change, the SiNP anode with GG binder can hold the capacity of 1000 mAh g^{-1} over 930 cycles at 1000 mA g^{-1}, which is 500 cycles longer than that with the SA binder. Thus, this study on GG as a binder opens a new binder-design perspective for Si anodes of LIBs.

4. Experimental Section

SiNPs were purchased from Alfa Aesar (Tianjin, China) and applied as active material without any further treatment. The morphology and composition of the SiNPs were characterized by SEM (HITACHI S-4800), XRD (Philips X'Pert Pro Super X-ray diffractometer, Cu-Ka radiation), and TEM (JEM 2100). The specific surface area of the SiNPs was obtained by the BET method using N_2 adsorption and desorption isotherms on a Micrometrics Tristar 3000 system.

Viscosity tests of the GG binder (Hongjian, Shanghai, China) and the SA binder (Maichao, Shanghai, China) were performed on a NDJ–5S viscosity tester (Changji, Shanghai, China) using 1.7 wt% GG and SA water solutions at 30 °C. Vickers hardness tests of the GG binder and the SA binder were carried out on a MHV–20002C stiffness tester (Taiming, Shanghai, China) under the conditions force = 25 gf and dwell = 15 s. For Vickers hardness tests, GG and SA were stirred in deionized water untill complete swelling and subsequently coated onto glass sheets. After drying at 50 °C for 12 h to form films, the binders were dried at 80 °C for 12 h in a vacuum oven for testing. FTIR spectra were recorded on a FTIR spectrophotometer (Nicolet 330) over the range of 4000–400 cm^{-1} using KBr pellets. TGA (TG 209-F1) measurements were performed in air between 30 and 800 °C at a heating speed of 10 °C min^{-1}. To study the binding strength between binders and SiNPs, the binder/Si blends with a mass ratio of 2:3 were stirred in deionized water to form homogeneous slurries and then dried at 50 °C for 6 h under draft condition and 80 °C for 12 h in a vacuum oven. Half of each sample was collected for TGA "before washing" and the other half underwent stirring for TGA "after washing". For the washing experiment, the dried binder/Si sample was vigorously stirred in deionized water for 1 h and collected by centrifugation. After repeating the above procedure 3 times, the binder/Si blend was dried at 80 °C for 12 h in a vacuum oven for TGA.

To prepare the working electrode of a coin cell, the active material, conductive additive, and binder (53:18:29 or 70:15:15 by weight) were stirred into a homogeneous slurry. In this study, the conductive additive was acetylene black. The obtained slurry was coated onto pure copper foil and dried in a vacuum oven at 80 °C for 12 h. The loading of SiNPs for charge-discharge cycling test was typically 0.2–0.3 mg cm^{-2} or 1.1 mg cm^{-2}. After drying, the working electrode was assembled, in an argon glove box, into a 2025 coin cell using lithium metal foil as the counter electrode and microporous Celgard 2400 membrane as the separator. 1 mol L^{-1} $LiPF_6$ in ethylene carbonate, diethyl carbonate and dimethyl carbonate (1:1:1 by volume) with 2 wt% vinylene carbonate and 10 wt% fluoroethylene carbonate was used as the liquid electrolyte solution (TINCI, Guangzhou, China). Galvanostatic cycling tests were carried out at room temperature on a LAND battery test system (Wuhan, China) between 0.01 and 1.2 V. In cycle performance test with the lithium insertion capacity limited to 1000 mAh g^{-1}, the cell was discharged untill the capacity reached 1000 mAh g^{-1} or the voltage reached 0.01 V, then charged to 1.2 V. CV tests were carried out between 0.01 and 3.0 V with a scanning rate of 0.2 mV s^{-1} on a CHI660D electrochemical workstation (Chenhua, Shanghai, China). EIS was acquired on a potentiostat (PARSTAT 2263) over a frequency range from 100 kHz to 0.01 Hz with an ac amplitude of 5 mV.

Supporting Information

Supporting Information is available from the Wiley Online Library or from the author.

Acknowledgements

This work was financially supported by Natural Science Foundation of China (NSFC) (Grant Nos. 21373008, 21321062, and 21273184).

Received: February 11, 2015
Revised: April 8, 2015
Published online: May 12, 2015

[1] Y. K. Jeong, T. Kwon, I. Lee, T. S. Kim, A. Coskun, J. W. Choi, *Nano Lett.* **2014**, *14*, 864.
[2] H. Wu, G. Yu, L. Pan, N. Liu, M. T. McDowell, Z. Bao, Y. Cui, *Nat. Commun.* **2013**, *4*, 1.
[3] B. Koo, H. Kim, Y. Cho, K. T. Lee, N. S. Choi, J. Cho, *Angew. Chem. Int. Ed.* **2012**, *51*, 8762.
[4] S. Chen, P. Bao, X. Huang, B. Sun, G. Wang, *Nano Res.* **2014**, *7*, 85.
[5] X. Zhao, X. Rui, W. W. Zhou, L. Tan, Q. Yan, Z. Lu, H. H. Hng, *J. Power Sources* **2014**, *250*, 160.
[6] Y. Hwa, W. S. Kim, B. C. Yu, J. H. Kim, S. H. Hong, H. J. Sohn, *J. Electroanal. Chem.* **2014**, *712*, 202.
[7] X. Zhou, Y. X. Yin, L. J. Wan, Y. G. Guo, *Chem. Commun.* **2012**, *48*, 2198.
[8] Z. Wen, G. Lu, S. Cui, H. Kim, S. Ci, J. Jiang, P. T. Hurley, J. Chen, *Nanoscale* **2014**, *6*, 342.
[9] L. F. Cui, Y. Yang, C. M. Hsu, Y. Cui, *Nano Lett.* **2009**, *9*, 3370.
[10] A. Gohier, B. Laïk, K. H. Kim, J. L. Maurice, J. P. P. Ramos, C. S. Cojocaru, P. T. Van, *Adv. Mater.* **2012**, *24*, 2592.
[11] W. J. Zhang, *J. Power Sources* **2011**, *196*, 13.
[12] M. H. Ryou, J. Kim, I. Lee, S. Kim, Y. K. Jeong, S. Hong, J. H. Ryu, T. S. Kim, J. K. Park, H. Lee, J. W. Choi, *Adv. Mater.* **2013**, *25*, 1571.
[13] A. Magasinski, B. Zdyrko, I. Kovalenko, B. Hertzberg, R. Burtovyy, C. F. Huebner, T. F. Fuller, I. Luzinov, G. Yushin, *ACS Appl. Mater. Interfaces* **2010**, *2*, 3004.
[14] J. S. Bridel, T. Azals, M. Morcrette, J. M. Tarascon, D. Larcher, *Chem. Mater.* **2010**, *22*, 1229.
[15] I. Kovalenko, B. Zdyrko, A. Magasinski, B. Hertzberg, Z. Milicev, R. Burtovyy, I. Luzinov, G. Yushin, *Science* **2011**, *334*, 75.
[16] J. Liu, Q. Zhang, Z. Y. Wu, J. H. Wu, J. T. Li, L. Huang, S. G. Sun, *Chem. Commun.* **2014**, *50*, 6386.
[17] J. Song, M. Zhou, R. Yi, T. Xu, M. L. Gordin, D. Tang, Z. Yu, M. Regula, D. Wang, *Adv. Funct. Mater.* **2014**, *24*, 5904.
[18] G. Liu, S. Xun, N. Vukmirovic, X. Song, P. O. Velasco, H. Zheng, V. S. Battaglia, L. Wang, W. Yang, *Adv. Mater.* **2011**, *23*, 4679.
[19] M. Wu, X. Xiao, N. Vukmirovic, S. Xun, P. K. Das, X. Song, P. O. Velasco, D. Wang, A. Z. Weber, L. W. Wang, V. S. Battaglia, W. Yang, G. Liu, *J. Am. Chem. Soc.* **2013**, *135*, 12048.
[20] D. E. Fenton, J. M. Parker, P. V. Wright, *Polymer* **1973**, *14*, 589.
[21] F. S. Li, Y. S. Wu, J. Chou, M. Winter, N. L. Wu, *Adv. Mater.* **2015**, *27*, 130.
[22] A. M. Stephan, *Eur. Polym. J.* **2006**, *42*, 21.
[23] Y. T. Kim, E. S. Smotkin, *Solid State Ionics* **2002**, *149*, 29.
[24] K. M. Abraham, Z. Jiang, B. Carroll, *Chem. Mater.* **1997**, *9*, 1978.
[25] M. George, T. E. Abraham, *Int. J. Pharm.* **2007**, *335*, 123.
[26] Y. S. R. Krishnaiah, S. Satyanarayana, Y. V. R. Prasad, S. N. Rao, *Int. J. Pharm.* **1998**, *171*, 137.
[27] M. Velimirovic, H. Chen, Q. Simons, L. Bastiaens, *J. Contam. Hydrol.* **2012**, *1*, 142.
[28] Y. N. Sudhakar, M. Selvakumar, D. K. Bhat, *Mater. Sci. Eng. B* **2014**, *180*, 12.
[29] D. Mudgil, S. Barak, B. S. Khatkar, *Int. J. Biol. Macromol.* **2012**, *50*, 1035.
[30] U. S. Vogl, P. K. Das, A. Z. Weber, M. Winter, R. Kostecki, S. F. Lux, *Langmuir* **2014**, *30*, 10299.
[31] P. Hobza, Z. Havlas, *Chem. Rev.* **2000**, *100*, 4253.
[32] M. Abdallah, *Port. Electrochim. Acta* **2004**, *22*, 161.
[33] P. Roy, P. Karfa, U. Adhikari, D. Sukul, *Corros. Sci.* **2014**, *88*, 246.
[34] M. Q. Li, M. Z. Qu, X. Y. He, Z. L. Yu, *Electrochim. Acta* **2009**, *54*, 4506.
[35] B. R. Lee, S. J. Kim, E. S. Oh, *J. Electrochem. Soc.* **2014**, *161*, A2128.